Pump plenum pressure dependence on divertor plasma parameters and magnetic geometry in the DIII-D tokamak

R. Maingi[a], J.G. Watkins[b], M.A. Mahdavi, L.W. Owen[a]
General Atomics, San Diego, California

[a] Oak Ridge National Laboratory, Oak Ridge, Tennessee
[b] Sandia National Laboratories, Albuquerque, New Mexico

United States of America

Abstract. A first-flight neutral transport model to describe the dependence of pump plenum neutral pressure on plasma parameters and magnetic geometry is presented. It is shown that the model is in excellent agreement with neutral pressure data from a low recycling DIII-D tokamak discharge. It is also shown that the main contribution to plenum pressure arises from the part of the ion particle flux profile which is closest to the plenum entrance. This work illustrates the sufficiency of a simple model in divertor plenum hardware design studies to maximize particle exhaust for density control.

Particle control is necessary for both present day fusion experiments and future power plants. Sustainment of these high performance plasma regimes requires density control [1, 2], and a power producing reactor will require exhaust of the helium ash byproduct. The two primary techniques used to enable particle control in present day tokamaks are wall conditioning techniques [3] and in-vessel pumping.

In-vessel pumping is usually accomplished in diverted tokamaks by the implementation of a turbopumping or cryopumping system installed in conjunction with a pump plenum and baffle system [1, 4–6]. The purpose of the plenum is to enhance the neutral particle density near the pumps by reducing the probability of neutral leakage back into the main plasma; in addition, the plenum must protect the pumps from contact with hot plasma or energetic neutrals. It has been demonstrated that a pump plenum and baffle system can indeed be designed to compress neutrals inside the plenum. For example, the DIII-D lower pump plenum neutral pressure increases strongly as the divertor outer strike point (OSP) is moved close to the plenum opening [1, 7–9]. The utility of divertor pumping has been demonstrated by enabling density control [1, 10] and wall deuterium inventory control [1, 11] in H mode plasmas.

Design of the plenum is crucial in optimization of the pumping system and is commonly done [12] with detailed 2-D edge plasma transport calculations coupled to 2-D or 3-D Monte Carlo neutral transport calculations. These calculations are both time consuming and suffer from uncertainties arising from the fact that the number of free parameters far exceeds the number of experimental constraints. To facilitate the design of future pump plenum openings for DIII-D, a model has been developed to relate the pump plenum neutral pressure to the divertor plasma parameters and the geometry of the OSP relative to the plenum opening. The goal of our model is to reproduce the measured plenum pressure dependence on OSP location by using the measured outer divertor plate density, temperature and parallel particle flux ($n_e^{div}(r)$, $T_e^{div}(r)$ and $\Gamma_i^{\|}(r)$, respectively) and a simple approximation for neutral transport into the pump plenum and neutral escape out of the plenum. The approximation used for neutral transport into the plenum consists of two probabilities: (a) the geometric solid angle of the plenum to first-flight recycled neutrals, $F(r)$; (b) the transmission probability that neutrals heading towards the plenum are not ionized prior to entering the plenum, $T(r)$. This simple technique is essentially a first-flight neutral transport model in that it neglects charge exchange contributions to the plenum pressure. It will be shown that this model produces excellent agreement with measurements from the DIII-D tokamak. We note here that this model has similarities to previous models for plenum pressure, for both pump limiters [13] and divertors [14]. The key difference is that we use experimentally measured divertor plasma profiles and time dependent magnetic equilibrium reconstructions as inputs. A description of the model and comparisons with data are given below.

 ©1999, IAEA, Vienna

The geometry of the lower divertor in DIII-D is shown in Fig. 1 and the geometry used for the pump plenum model is shown schematically in Fig. 2. The boundary of the plenum is defined in this model by a critical radial location R_{cr}. The neutrals which are transported past this critical radius are considered to be inside the plenum. This model effectively treats the entrance of the plenum as an aperture at R_{cr} with a given height H.

The neutral pressure in the plenum at a given OSP radius R_{OSP} is given by

$$P_0^{plen}(R_{OSP}) = \frac{I_0^{plen}(R_{OSP})}{7 \times 10^{19}(S_{pump} + C)} \quad (1)$$

where P_0^{plen} is the plenum pressure (torr), I_0^{plen} the neutral 'current' entering the plenum (integrated over target ion flux profile) (particles/s), S_{pump} the pumping speed (L/s) and C the molecular back conductance out of the plenum (L/s). From in situ calibrations, $S_{pump} \sim 30$ m^3/s (if the cryopump is on and $P_0^{plen} < 1$ mtorr) and $C \sim 40$ m^3/s ($P_0^{plen} < 4$ mtorr) for thermal, molecular D_2. Note the 7×10^{19} factor in Eq. (1) converts from amperes to torr L/s. The neutral 'current' transported into the pump plenum is a function of R_{OSP} and is given formally by

$$I_0^{plen}(R_{OSP}) = \int_{R_{min}}^{R_{max}} \Gamma_0(r) F(r) T(r) 2\Pi R_m(r)\, dr \quad (2)$$

where $\Gamma_0(r)$ is the neutral flux radial profile, $F(r)$ the geometric solid angle of plenum opening, $T(r)$ the probability that neutrals will not be ionized during transport into the plenum, R_{min} and R_{max} the limits of outer divertor particle flux profile, and R_m the major radius.

The limits of integration are determined as follows: R_{max} is taken to be the maximum flux surface radius that does not intercept the front face of the plenum structure. The face of the plenum entrance is at 1.692 m; however, the poloidal flux surfaces in DIII-D intercept the target with an incidence angle ~45°. We use $R_{max} = 1.72$ m based on typical equilibrium magnetic reconstructions. Note that this means R_{max} actually exceeds R_{cr}, due to the flux surface geometry. To allow for the contribution of neutrals originating from the private flux region (PFR), R_{min} must be set to a few PFR particle flux radial e-folding lengths less than R_{OSP}. Typically $\lambda_{PFR}^{\Gamma_\parallel} \sim 1$–1.5 cm; hence, we use $R_{min} = R_{OSP} - 8$ cm for simplicity.

We need to relate the unknowns $\Gamma_0(r)$, $F(r)$ and $T(r)$ to geometry and measurable quantities in order

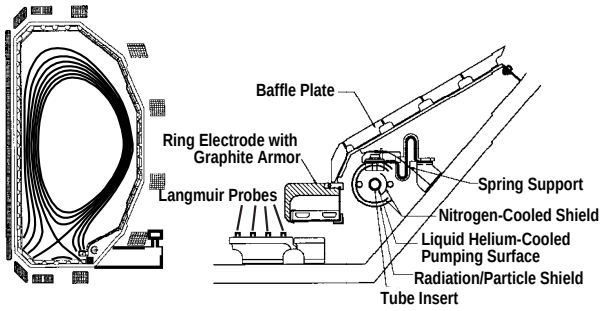

Figure 1. DIII-D poloidal cross-section and cryopump diagram.

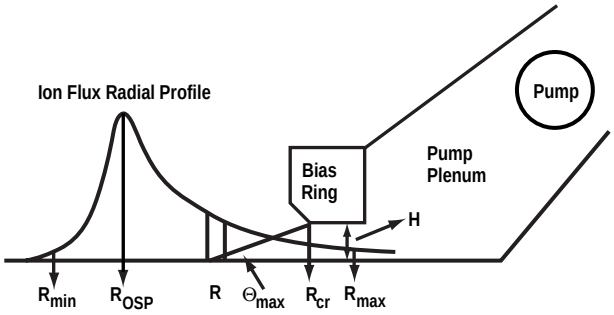

Figure 2. Schematic representation of pump plenum entrance.

to solve Eq. (2). The neutral recycling flux profile at the target $\Gamma_0(r)$ is comprised of Franck–Condon neutral flux Γ_{FC} and fast reflected neutral flux Γ_{RE}, i.e. $\Gamma_0(r) = \Gamma_{FC}(r) + \Gamma_{RE}(r)$. These can be related to the ion flux radial profile, parallel to the total magnetic field, $\Gamma_i^{\parallel}(r)$ by

$$\Gamma_{FC}(r) = (1 - R_n)\Gamma_i^{\parallel} \sin[\Theta_B(r)] \quad (3a)$$

$$\Gamma_{RE}(r) = R_n \Gamma_i^{\parallel} \sin[\Theta_B(r)] \quad (3b)$$

where R_n is the energetic particle reflection coefficient and $\Theta_B(r)$ the incidence angle of the magnetic field on the floor ($= \tan^{-1}[B_z(r)/B_\phi(r)]$). We use $R_n = 0.25$, based on the fractal TRIM modelling code for rough graphite surfaces [15]. In fact the Franck–Condon flux originates from the target largely as molecules, but these molecules have a short dissociation mean free path λ_{diss} for our divertor parameters (0.4 mm $< \lambda_{diss} <$ 2 mm); the dissociation process creates neutrals at the Franck–Condon energy of ~3 eV. $\Gamma_i^{\parallel}(r)$ is obtained from divertor Langmuir probe analysis, discussed later.

The probability that recycled neutrals will be transported towards the pump plenum $F(r)$ is given

by the solid angle of the plenum opening at the point of neutral origin:

$$F(r) = \frac{\int_0^{\Theta_{max}} I(\Theta) dS(\Theta)}{\int_0^{\Pi} I(\Theta) dS(\Theta)} \quad (4)$$

where $I(\Theta)$ is the poloidal distribution of recycled neutral current and $dS(\Theta)$ the differential area subtended by the plenum entrance ($=2\Pi R_m \sin(\Theta)\, d\Theta$).

The maximum acceptance angle for a neutral originating at major radius R is shown schematically in Fig. 2. For $R < R_{cr}$, $\Theta_{max} = \tan^{-1}[H/(R - R_{cr})]$; for $R > R_{cr}$, $\Theta_{max} = \tan^{-1}[H/(R - R_{cr})] + 180°$, where $H = 0.027$ m and $R_{cr} = 1.692$ m for the DIII-D lower pump plenum hardware. On the basis of the fractals TRIM modelling [15] of deuterium recycling off rough graphite surfaces, both Franck–Condon and fast reflected species are assumed to have an isotropic poloidal distribution. In this case, Eq. (4) has an analytic solution,

$$F(r) = \frac{\int_0^{\Theta_{max}} \sin(\Theta)\, d\Theta}{2} = \frac{1 - \cos[\Theta_{max}(r)]}{2}. \quad (5)$$

Next we compute the SOL ionization probability, which attenuates the neutral flux aimed towards the pump plenum. This attenuation can be computed from the neutral flux continuity equation

$$\frac{d\Gamma_0(r)}{dr} = -n_e(r) n_0(r) \langle \sigma v \rangle_{EII}(r) = -\frac{n_e(r)\Gamma_0(r)\langle \sigma v \rangle_{EII}(r)}{v_0} \quad (6)$$

where $v_0 = \sqrt{2E_0/m_0}$, E_0 is the assumed neutral kinetic energy and m_0 the neutral mass ($=3.34 \times 10^{-27}$ kg).

The solution to Eq. (6) yields the transmission factor $T(r)$,

$$T(r) \equiv \frac{I_0^{plen}(R_{max})}{I_0^{plen}(R)} = \exp\left[\frac{-1}{v_0}\left(\int_R^{R_{max}} n_e(r)\langle \sigma v \rangle_{EII}(r)\, dr\right)\right]. \quad (7)$$

The fast reflected neutrals are assumed to have a mean energy of $2.5T_e$, resulting from an energy reflection coefficient [15] of 0.5 and an assumed ion impact energy of $3.5T_e + 1.5T_i \sim 5T_e$. The Franck–Condon neutrals have a mean energy of 3 eV. The spatial dependence of the $\langle \sigma v \rangle_{EII}(r)$ in Eq. (7) originates from its T_e dependence and the spatial profile of T_e. An analytic approximation [16] for the T_e dependence of the electron impact ionization (EII) reaction rate parameter is used (T_e in eV):

$$\langle \sigma v \rangle_{EII}(r) \approx \frac{3 \times 10^{-16} T_e^2(r)}{3 + 0.01 T_e^2(r)}\ (\mathrm{m}^3\ \mathrm{s}^{-1}). \quad (8)$$

Equations (1)–(8) can be solved with divertor target profiles for $n_e^{div}(r)$, $T_e^{div}(r)$ and $\Gamma_i^{\parallel}(r)$ and magnetics reconstruction. The $n_e^{div}(r)$, $T_e^{div}(r)$ and $\Gamma_i^{\parallel}(r)$ profiles are measured by sweeping the OSP over Langmuir probes embedded [17] in the target (Fig. 1). This technique produces a more spatially resolved profile than that using multiple probes at a single time slice because the probes are physically separated by 3 cm. However, this technique requires an assumption that the target $n_e^{div}(r)$, $T_e^{div}(r)$ and $\Gamma_i^{\parallel}$ profiles are constant relative to the OSP during the OSP sweep. Mapping of the time dependence of the divertor parameter measurements yields spatial profiles of $n_e^{div}(r)$, $T_e^{div}(r)$ and $\Gamma_i^{\parallel}(r)$ relative to the OSP. These spatial profiles are fitted with up to three different exponential scale lengths, two on the SOL side of the separatrix and one on the PFR side. The fitted profiles are then used in the calculation of plenum pressure.

The evaluated discharge (No. 95255) was a lower single null configuration with $I_p = 1.4$ MA, $B_t = -2.0$ T, ion ∇B drift towards the X point and NBI power ~4.7 MW. This H mode discharge had an approximately constant line averaged density of 5×10^{19} m^{-3} during the OSP sweep and the cryopump was inactive. The divertor target profiles were reconstructed from four Langmuir probes: 4–1, $R = 1.580$ m; 4–2, $R = 1.608$ cm; 4–3, $R = 1.635$ cm; 4–4, $R = 1.663$ cm. These profiles (shown in Fig. 3) all peak within 1 cm of the OSP, which is the nominal uncertainty of the OSP location from magnetics reconstruction. Note that the profiles obtained from the different probes largely overlap, which indicates that the assumption of static profiles during the OSP sweep used above is justified.

The plenum pressure is computed for a range of OSP locations; in each case, the $n_e^{div}(r)$, $T_e^{div}(r)$ and $\Gamma_i^{\parallel}$ profiles relative to the OSP are held fixed. Time dependent magnetics reconstructions with the EFITD code [18] are used, i.e. each OSP location in the calculation range uses the magnetic geometry with the closest actual OSP location from the discharge. This means that $\Theta_B(r)$ varies over the OSP calculation range in the same way that it varies experimentally during the OSP sweep. It is

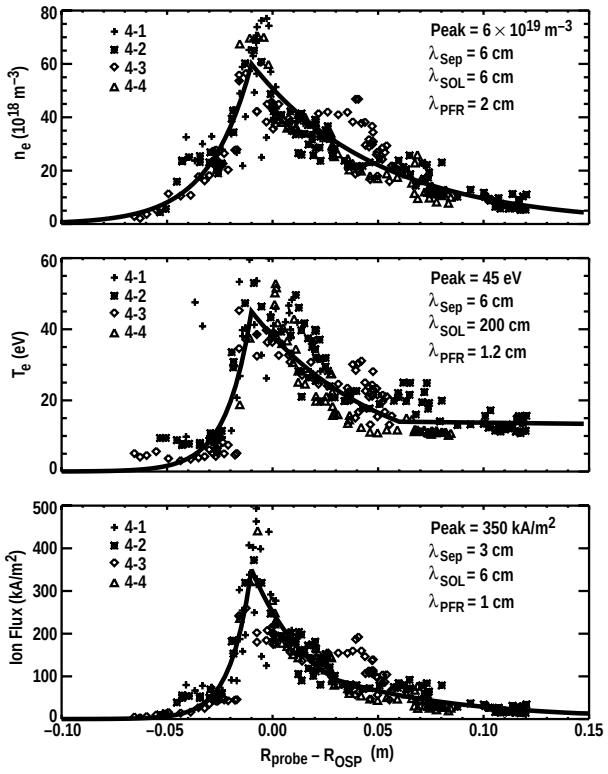

Figure 3. Profiles of $n_e^{div}(r)$, $T_e^{div}(r)$ and $\Gamma_i^{\parallel}(r)$ from Langmuir probe data, for discharge 95255: $I_p = 1.4$ MA, $B_t = -2.0$ T, $P_{NBI} = 4.7$ MW, lower single null divertor. The spatial profiles relative to the separatrix are obtained by translating time dependent profiles obtained during an OSP sweep. λ_{Sep} is the e-folding length very close to the separatrix (SOL side), λ_{SOL} is the e-folding length further in the SOL and λ_{PFR} is the e-folding length in the private flux region.

important to use the time dependent $\Theta_B(r)$ because $\Theta_B(r)$ increases at higher major radius (higher B_z, lower B_ϕ).

Results of the computed plenum pressure are compared with data in Fig. 4 for discharge 95255. Two model predictions are shown: the solid curve allows the divertor ion current to vary as indicated by the magnetics and the assumption that the profiles do not change during the OSP sweep (variable ion current model). The dashed curve fixes the ion current at the average value computed from the variable ion current model; this is done by adjusting the peaks of the $\Gamma_i^{\parallel}$ and n_e^{div} profiles at each OSP location while keeping the scale lengths fixed (fixed ion current model). Thus, the fixed ion current model is more indicative of the impact of the geometric aspect of OSP changes on pressure buildup, while the variable ion current model includes the effect of

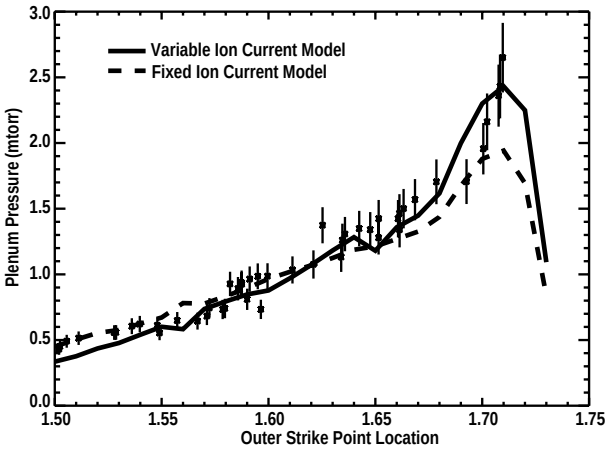

Figure 4. Computed pressure from both variable and fixed ion current models compared with data versus OSP position for discharge 95255.

the magnetic field target incidence angle changing with major radius.

Both models for ion current are in excellent agreement with the computed peak pressure as shown in Fig. 4. Qualitatively the plenum neutral pressure is highest when the OSP is close to the plenum opening because the solid angle factor $F(r)$ is the highest. In other words, the geometric dependence of $F(r)$ is the strongest variable in Eq. (2). Note that the computed plenum pressure is most sensitive to the $\Gamma_i^{\parallel}$ and n_e^{div} profiles. T_e^{div} is used only in the calculation of the transmission factor $T(r)$, and this factor is almost unity for the discharge studied because the ionization mean free path λ_{ion} is relatively long under these conditions ($\lambda_{ion} \leq 2$, 10 cm for Franck–Condon particles and fast reflected particles, respectively).

It is interesting to note that both models predict the plenum pressure quite accurately even when the OSP is far away from the plenum opening, for example $R < 1.60$ m. It is under these conditions that charge exchange/diffusion might affect the neutral transport into the plenum. However, it can be inferred from the excellent agreement at small OSP locations in Fig. 4 that either the magnitude of this effect is small or that charge exchange/diffusion of neutrals into the plenum acceptance cone is approximately balanced by transport of neutrals out of the acceptance cone.

Note that both models predict a rapid fall-off of neutral pressure as R_{OSP} exceeds R_{max}. This fall-off in neutral pressure has been observed experimentally in other discharges with larger OSP sweeps; unfortunately, the OSP in this discharge was swept out only

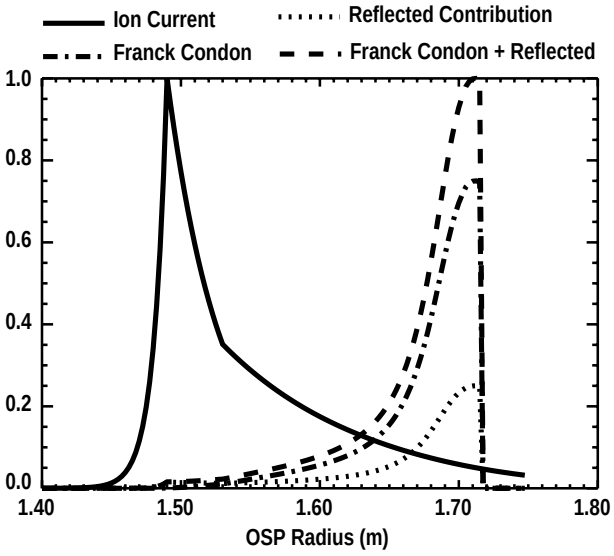

Figure 5. Normalized particle current profile versus major radius when the OSP is at $R = 1.50$ m. The dashed curves show the model calculations for the normalized contributions to the plenum pressure as a function of the neutral origination.

to $\sim R = 1.71$ m. Physically this reduction in the neutral pressure occurs because the ion flux 1–2 cm on the SOL side of the separatrix is scraped off by the side of the bias ring which defines the plenum opening. The neutrals along this trajectory cannot contribute to the first flight neutral flux entering the plenum. These neutrals could contribute indirectly to the plenum flux by ionization in the SOL and subsequent flow to the target. If this were a large effect, an increase in the peak ion flux would be observed when the OSP was moved into the plenum entrance. However, such an increase of the peak ion flux as R_{OSP} approaches R_{max} has not been found by the Langmuir probes in this or other similar discharges. Thus, it can be concluded that the plenum pressure contribution of neutrals recycling off the face of the plenum opening is indeed negligible for the discharge conditions.

It is instructive to examine where most of the neutrals that contribute to the plenum pressure originate from, as well as which neutral energy population (Franck–Condon or reflected) is the larger contributor to the pressure. Figure 5 shows the results of a calculation with the OSP at 1.50 m. The normalized ion current profile ($I(R_m) = 2\Pi R_m \Gamma_i^{\parallel}(R_m) \sin[\Theta_B(R_m)]$) shown in Fig. 5 peaks 1 cm on the private flux region side of the OSP, consistent with the $\Gamma_i^{\parallel}(r)$ profile in Fig. 3. Also shown are the (normalized) calculated contributions of neutrals to the plenum current from Franck–Condon neutrals, i.e. $\Gamma_{FC}(R_m)F(R_m)T_{FC}(R_m)2\Pi R_m$, and reflected neutrals, i.e. $\Gamma_{RE}(R_m)F(R_m)T_{RE}(R_m)2\Pi R_m$. Note that even though the ion current profile peaks 20 cm away from the plenum opening at $R = 1.692$ m, most of the contribution to the plenum pressure originates from neutrals born near the plenum entrance. This occurs primarily because the solid angle factor $F(R_m)$ increases strongly as R_m approaches R_{cr}. Owing to the relatively long ionization mean free path in this low recycling discharge, the neutrals close to the plenum entrance have negligible minor plasma attenuation, i.e. $T_{RE} \sim T_{FC} \sim 1$ as R_m approaches R_{cr}. Thus, the total Franck–Condon contribution (chain curve, Fig. 5) exceeds the reflected particle contribution (dotted curve), roughly by $(1 - R_n)/R_n \sim 3$.

It is noteworthy to contrast the sharp dependence of DIII-D's plenum neutral pressure on OSP location with other tokamaks at this point. Both JET [19, 20] and Alcator C-Mod [21] have reported a weak dependence of the plenum pressure on the plenum opening location. It was concluded in Ref. [14] that DIII-D's plenum pressure was primarily linked to first flight neutrals, whereas both Alcator C-MOD and JET have charge exchange neutrals as the dominant contributor to plenum pressure. While we cannot confirm the conclusions about JET and Alcator C-MOD, our model supports the conclusion of the origin of DIII-D's plenum pressure.

We have shown that a simple recycling and neutral transport model can be used to accurately predict plenum pressure as a function of geometry and target plate plasma parameters. This model clearly applies to discharges with a long divertor ionization mean free path for neutrals; the usage of this model in the intermediate or short mean free path limit requires more study. This model has since been used to corroborate the design of the additional hardware planned for installation in the private flux region and the inner wall of DIII-D, which began in August 1999.

Acknowledgements

This is a report of work supported by the USDOE under Contract Nos DE-AC03-99ER54463, DE-AC05-96OR22464 and DE-AC04-94AL85000.

Note added in proof. R. Maingi has recently moved to: Princeton Plasma Physics Laboratory, Princeton University, Princeton, New Jersey, USA.

References

[1] Mahdavi, M.A., et al., in Fusion Engineering (Proc. 15th Symp. Hyannis, 1993), Vol. 2, IEEE, Piscataway, NJ (1994) 597.

[2] Lazarus, E.A., et al., in Plasma Physics and Controlled Nuclear Fusion Research 1994 (Proc. 15th Int. Conf. Seville, 1994), Vol. 1, IAEA, Vienna (1995) 609.

[3] Winter, J., Plasma Phys. Control. Fusion **36** (1994) B263.

[4] Schaubel, K., et al., in Fusion Technology (Proc. 18th Symp. Karlsruhe, 1994), Elsevier, Amsterdam and New York (1995) 347.

[5] Smith, J., Baxi, C., Reis, E., Sevier, L., Fusion Technol. **21** (1992) 1658.

[6] Menon, M.M., et al., Fusion Technol. **22** (1992) 356.

[7] Mahdavi, M.A., et al., in Plasma Physics and Controlled Nuclear Fusion Research 1990 (Proc. 13th Int. Conf. Washington, DC, 1991), Vol. 1, IAEA, Vienna (1991) 335.

[8] Klepper, C.C., et al., Nucl. Fusion **33** (1993) 533.

[9] Maingi, R., et al., J. Nucl. Mater. **220–222** (1995) 320.

[10] Mahdavi, M.A., et al., in Controlled Fusion and Plasma Physics (Proc. 20th Eur. Conf. Lisbon, 1993), Vol. 17C, Part I, European Physical Society, Geneva (1993) 647.

[11] Maingi, R., et al., Nucl. Fusion **36** (1996) 245.

[12] Fenstermacher, M.E., et al., J. Nucl. Mater. **220–222** (1995) 330.

[13] Corbett, W.J., et. al., Nucl. Fusion **31** (1991) 1067.

[14] Loarte, A., et al., in Controlled Fusion and Plasma Physics (Proc. 24th Eur. Conf. Berchtesgaden, 1997), Vol. 21A, Part III, European Physical Society, Geneva (1997) 1049.

[15] Ruzic, D.N., Chiu, H.K., J. Nucl. Mater. **162–164** (1989) 904.

[16] Braams, B.J., Computational Studies in Tokamak Equilibrium and Transport, PhD Thesis, Univ. of Utrecht (1986).

[17] Buchenauer, D., Hsu, W.L., Smith, J.P., Hill, D.N., Rev. Sci. Instrum. **61** (1990) 2873.

[18] Lao, L.L., et al., Nucl. Fusion **25** (1985) 1611.

[19] Ehrenberg, J.K., et al., in Controlled Fusion and Plasma Physics (Proc. 22nd Eur. Conf. Bournemouth, 1995), Vol. 19C, Part I, European Physical Society, Geneva (1995) 309.

[20] Saibene, G., et al., ibid., Part II, p. 121.

[21] Niemczewski, A., et al., Nucl. Fusion **37** (1997) 151.

(Manuscript received 23 April 1999
Final manuscript accepted 22 July 1999)

E-mail address of R. Maingi:
rmaingi@pppl.gov

Subject classification: J2, Tm; L2, Tm